UNIVERSITY OF CALIFORINA,

IRVINE

Strengthening and softening in nanocrystalline nickel

THESIS

submitted in partial satisfaction of the requirements
for the degree of

MASTER OF SCIENCE

in Materials Science and Engineering

by

ANNA TORRENTS CABESTANY

Thesis Committee:
Professor Farghalli A. Mohamed, Chair
Professor James C. Earthman
Professor Daniel R. Mumm

2007

The thesis of Anna Torrents Cabestany is approved:

_____

_____

_____
Committee Chair

University of California, Irvine
2007

TABLE OF CONTENTS

Page

LIST OF FIGURES

Page

LIST OF TABLES

Page

ACKNOWLEDGMENTS

I would like to express my gratitude to my academic advisor, Professor Farghalli A. Mohamed, for providing me the opportunity to pursue a M.S degree in Materials Science and Engineering.

I also acknowledge Professor James C. Earthman and Professor Daniel R. Mumm for serving as committee members on my thesis committee.

I owe special thanks to Dr. Manish Chauhan for his excellent technical assistance and advice. I would also like to thank graduate and undergraduate students in my group for their unselfish assistance, including Dr. Indranil Roy, Ms. Heather Yang, Ms. Linh Dinh and Mr. Kelvin Cheung.

The author would like to acknowledge the financial support from Balsells – Generalitat de Catalunya fellowship 2005-06.

ABSTRACT OF THE THESIS

Strengthening and softening in nanocrystalline nickel

By

Anna Torrents Cabestany

Master of Science in Materials Science and Engineering

University of California, Irvine, 2007

Professor Farghalli A. Mohamed, Chair

In the present investigation, hardness and Young's modulus of bulk electrodeposited nanocrystalline Ni having an average initial grain size of 20 nm were studied as a function of temperature. Hardness measurements were conducted at room temperature on specimens after annealing at different temperatures, ranging from 323 – 693 K for various annealing times. The results showed that the hardness of the material initially increased slightly with increasing annealing temperature and then decreased rapidly with increasing temperature above 500 K. It was suggested that the increase in hardness below 500 K was most likely due to the occurrence of substructural relaxation at non-equilibrium boundaries and the formation of annealing twins. Below 500 K, Young's modulus was shown to increase from 160 GPa to 250 GPa with increasing temperature; it remained constant at higher temperatures. Preferred orientation along (200) was observed in as-received samples. Thus, the increment in the Young's modulus can be attributed to a change in the preferential orientation along the (200) planes toward (111) with annealing temperature.

Chapter 1 : Introduction

In the last few decades, nanocrystalline (nc) materials such as Cu [1-4], Ag [3], Pd [1-5], Ni [6-12], and Ni-P [13, 14] have been widely used to study the Hall-Petch (HP) [15, 16] relationship. Some of these studies have reported the presence of a transition from grain size strengthening to softening ("inverse HP relation"), i.e. a decrease in hardness with decreasing grain size. While most of the hardness tests have been carried out on as prepared specimens at room temperature, little information on the effect of thermal annealing on hardness is available [10, 12, 13, 17].

Fougere *et al*. [17] reported an increased hardness with decreasing grain size for nc-Cu and nc-Pd when samples were annealed at 0.315 *Tm*, i.e. at 423 K and 569 K, respectively. Such strengthening was explained in terms of the reduction of porosity during annealing. Chen *et al*. [13] studied Ni-P hardness behavior after heat-treatment in a temperature range from 623 K to 873 K. They reported that hardening occurred below a critical temperature, located between 623 K and 673 K, followed by softening after annealing at higher temperature. They associated the increase of hardness with increasing annealing temperature to the formation of nano-crystals. Yang *et al*. [12] heat-treated nc-Ni samples at 573 K and 673 K for different holding times to produce a range of grain sizes from 30 μm to 30 nm. They reported that hardness increased with decreasing grain size within the whole grain size range examined, but the slope changed with decreasing grain size. Their increase in hardness was related to the dislocation density within the indented grains. Recent molecular dynamics simulation by Hasnaoui *et al*. [18] has

suggested that grain boundaries of as prepared nc-materials are often in a non-equilibrium state after processing and that as a result of thermal annealing, the grain boundaries and triple junction regions approach equilibrium (strengthening the material but reducing its ductility). The results by computer simulation are consistent with the experimental data reported by Wang *et al.* [10] for fully dense nc-Ni prepared by electrodeposition, whose grain size was about 15 nm.

Examination of the literature appears to show that most investigators agree that softening during annealing is related to grain growth. While explanations for strengthening mechanisms appear to be more diverse, the possible role of annealing twins as a mechanism that may enhances the strength of nc-materials, has not been considered.

In the present study, nc-Ni samples with an initial average grain size of 20 nm were annealed at different temperatures, ranging from 323 K to 693 K for two different holding times, i.e. 1 h and 25 h. The purpose of this work is two fold. Firstly, to provide more insight into the variation of hardness and Young's modulus values with grain size, and observe the effect of temperature / annealing on fully dense nc-Ni prepared by the electrodeposition technique. Secondly, to correlate the experimental data with recent thermal stability studies on nc-Ni at low temperature by M. Chauhan and F.A. Mohamed [19], and give a detail description of microstructure, mechanical properties and elastic properties of bulk nc-Ni within a wide range of temperatures.

Chapter 2 : Techniques

2.1 XRD – Integral Breadth Analysis [20]

The Integral Breadth (IB) method estimates the average crystallite size and the microstrain by XRD line broadening. Line broadening of Bragg's peaks is caused either by the small size of the diffracting grains or microstrain. Klug and Alexander [20] suggested that strain broadening may usually be approximated by a Gaussian function, whereas the effect of small crystallite size can be more closely represented as a Cauchy broadening profile. This relationship is represented by:

$$\frac{(\delta 2\theta)^2}{\tan^2\theta_0} = \frac{K\lambda}{L}\left(\frac{\delta 2\theta}{\tan\theta_0 \sin\theta_0}\right) + 16e^2 \qquad (1)$$

where $\delta 2\theta$ is in radians, λ is the wave length of Cu Kα, and *K* is a factor, being taken as 1. By plotting $(\delta 2\theta)^2/\tan^2\theta_0$ against $\delta 2\theta/\tan\theta_0 \sin\theta_0$ a linear relationship can be obtained. From the slope, $K\lambda/D$, and ordinate intercept, $16e^2$, the grain size and the micro-strain may be determined.

2.2 Microindentation [21]

The most common microindentation test is Vickers test (ASTM E92-82). The Vickers test uses a pyramidal indenter with a square base, made of diamond. The Vickers hardness (HV) is computed by the equation:

$$HV = \frac{2P\sin(\alpha/2)}{d^2} = \frac{1.8544P}{d^2}, \qquad (2)$$

where *P* is the applied load (in Kg), *d* is the average length of the diagonals (in mm), and α is the angle between the opposite faces of the indenter (136º). Some

considerations that should to be taken when performing Vickers test are: (a) the way in which the material behaves beneath the indenter affects the shape of the impression. Concave or convex curves of the square impression result in reading errors. (b) Microhardness varies with load and there is a tendency for the microhardness to increase (up to few grams); then the hardness value drops with load. (c) As with other hardness tests, the distance between indentation has to be greater than two and one-half times the length of the indentation diagonal, to avoid interaction between the work-hardening regions.

2.3 Nanoindentation [22, 23]

The two mechanical properties measured most frequently using load and depth sensing indentation techniques are the elastic modulus, *E*, and the hardness, *H*. The nanoindentation method used to calculate either hardness or Young's modulus is based on the method developed by Oliver and Pharr [22]. This method is in fact, a modification of the method obtained by Doerner and Nix [23] in 1986.

Depth-sensing instruments record the total penetration of the indenter into the sample, so a method for determining the elastic and plastic deformation is required. The nano-indenter is a triangular pyramid-shape diamond, called Berkovich, with the same area to depth ratio as the traditional Vickers pyramid.

During the loading stage then, the total penetration depth, *h*, is the summation of the elastic and plastic depth, which is used to determine the contact area. During the unloading stage, elastic recovery takes place, and thus the contact depth, h_c, can be determined by the unloading curve (see **Figure 1**). According to an elastic contact theory, Oliver and Pharr [22] demonstrated that at the maximum load, the

contact depth (h_c) can be calculated by the following equation:

$$h_c = h_{\max} - \varepsilon \frac{P_{\max}}{S} \tag{3}$$

where h_{max} is the total depth at the maximum load (P_{max}), ε is the indenter shape factor whose value for a conical indenter is 0.72 [22], and S is the stiffness of the material at P_{max}, which can be derived by the tangent at the maximum depth:

$$S = \left.\frac{dP}{dh}\right|_{h=h_{\max}} \tag{4}$$

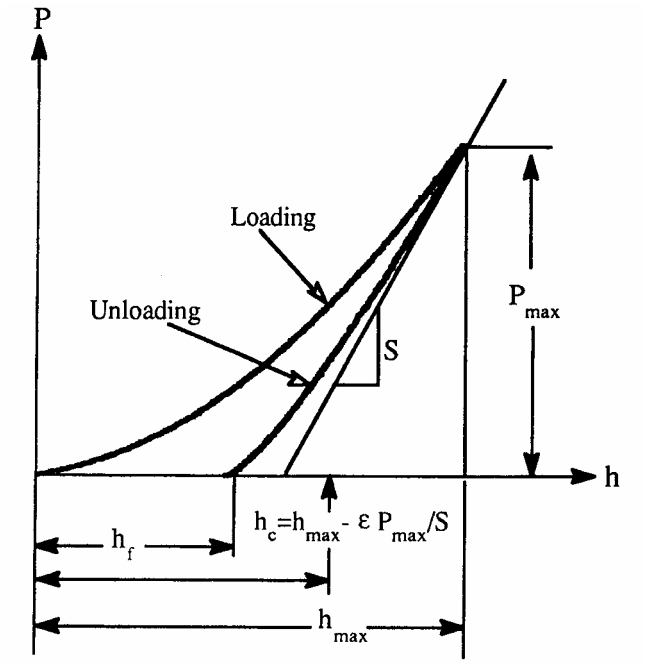

Figure 1 Typical nanoindenter loading and unloading curves.

Chapter 3 : Experimental procedure

3.1 Material and Processing

Electrodeposited (ED) nc-Ni of different grain sizes was used in the present investigation. The material was provided by two sources: (a) Integran Technologies Inc., Toronto, Canada in the form of 0.5 mm sheets with an initial grain size of 20 nm and 100 nm, and (b) Lawrence Livermore National Laboratory, CA in the form of 0.3 mm sheets with an initial grain size of 15 nm and 25 nm.

The chemical composition of as-received ED nc-Ni from the former source is shown in **Table 1**. Chemical analysis shows the presence of S and C impurities. The concentration of impurities is less than 0.1 wt.% and can be considered as interstitial type impurities. The presence of these kinds of impurities is associated with the use of additives such as coumarin and saccharin in the electrolyte bath.

Elements	**C**	Si	P	**S**	Cu	Co	B	**Ni**
Wt.%	**0.013**	<0.001	0.003	**0.058**	0.023	0.071	0.0091	**Balance**

Table 1 Chemical composition of electrodeposited nc-nickel

As-received nc-Ni samples of 15, 20, 25, and 100 nm, were characterized using X-ray diffraction (XRD) and TEM. Nc-Ni samples with an average grain size of 20 nm were annealed at nine different temperatures, ranging from 323 K to 693 K and two different annealing times, i.e. 1 hour and 25 hours. After annealing the samples were rapidly cooled in air and characterized using XRD to calculate the grain size. In order to compare the grain size results obtained using XRD, some samples were characterized using Transmission Electron Microscopy (TEM). Electron

Backscattered Diffraction (EBSD) was used to corroborate the TEM grain size values and obtain grain / coincidence site lattice (CSL) orientation maps. Because of the limitiation of EDSD technique, only those samples with grain size larger than 100 nm were analyzed.

All samples were mounted in cold mounts, using a mixer of a Buehler EPO-THIN low viscosity resin and its hardener (100:36). Mounts were polished using SiC papers of different grit sizes, starting with 600, 2400 and 4000, and alumina powder 0.05 μm was used for final polishing. Once polished, the samples were tested using microindentation and nanoindentation techniques to determine their hardness and Young's Modulus.

3.2 Characterization

3.2.1 XRD

Grain size measurements were conducted using X-ray diffraction (XRD). A Siemens D5000 diffractometer equipped with a graphite monochromator using copper K_α (λ = 0.15406 nm) radiations was used. General scans with a step size of 0.02 degree (2 θ) and with a step time of 2 seconds were used for grain size determination. The Integral breadth (IB) method [20] using five strong FCC Ni peaks ({111}, {200}, {220}, {311}, and {222}) was used after subtracting the instrumental broadening and $K_{\alpha 2}$ components.

3.2.2 TEM

Grain size and grain size distribution measurements were conducted using a Philips CM 20 TEM at 200 kV. The grain size was calculated applying the linear

intercept method, measuring the length for each grain along a set of X and Y directions. Samples were prepared by a combination of mechanical grinding and electro jet polishing. The polishing solution used was of the composition: 75% HNO_3 and 25% MeOH. A current of 8 V and 4 mA was used and the temperature was kept below 243 K.

3.2.3 EBSD

Grain size measurements and grain / coincidence site lattice (CSL) orientation maps were obtained using Zeiss Ultra 55 SEM with an acceleration voltage of 20 kV, and in which the HKL Flamenco Channel 5 hardware and software is interfaced. Measurements of orientation maps were performed with a step size of 30 nm. $\sum 3^n$ boundaries were analyzed using CSL statistic software. Sample preparation required a mechanical polishing, followed by electro-polishing at room temperature with a reading voltage of 8 V. The composition used was a mixture of: 20% H_2SO_4 and 80% MeOH.

3.3 Mechanical testing

Indentation testing was performed on a polished planar surface of nc-Ni samples using both microindenter and nanoindenter. While most of the tests were carried out on a microindenter, a nanoindenter was selectively used to measure the hardness and Young's Modulus and to verify the trends obtained from microindenter. The samples tested were annealed at different temperatures, varying from 323 – 693 K, for 1 hour and 25 hours. The reported results are the average values of more than ten indents on both testers.

3.3.1 Microindentation

Microindentation measurements were carried out at room temperature using a Buehler Microtester 5101 equipped with a square base diamond indenter, well known as a Vickers indenter. A load of 10, 50 and 200 g with a holding time of 20 s was applied. Although most of the tests were performed at 10 g load, (loads closer to those obtained from nanoindentation), 50 and 200 g loads were selectively used to check the trend.

3.3.2 Nanoindentation

Nanoindentation measurements were performed using an MTS Nanoindenter-XP model. A Berkovich (three sided pyramidal) indenter was used throughout these experiments. The area function for the diamond (the relationship between the projected contact area and contact depth) was calibrated by indentations into pure Ni from 0.5 – 200 mN. Indentations were depth controlled to 500 nm maximum penetration depth with a constant strain rate of 0.05 s^{-1}. All data were corrected for thermal drift and instrumental compliance in the instrument software and subsequently analyzed for the determination of Young's modulus (E) and hardness (H) using the Continuous Stiffness Method (CSM) procedure developed by Oliver and Pharr [22].

Chapter 4 : Results

4.1 Texture

4.1.1 As-received

Figure 2 provides a typical example for the XRD pattern of as-received nc-Ni with an average initial grain size of 20 nm. The XRD profile shows strong orientation in (111) followed by (200). In terms of relative peak intensity, the (200) planes of the experimental XRD profiles are much stronger, compared with the standard JCPDS pattern (04-0850). ($I_{200/111}$= 0.75 > $I_{200/111}$= 0.46). This observation reveals a preferred texture around (200) planes oriented predominantly in the as-received ED nc-Ni. These results agree with those previously reported on the microstructural characterization of as electrodeposited nc-Ni by Chauhan and Mohamed [19], although an extra peak in the XRD profile was not found.

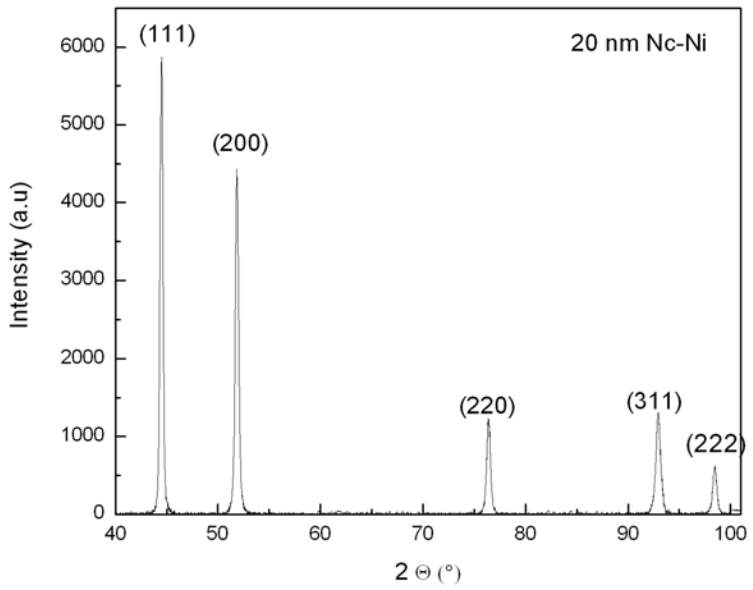

Figure 2 XRD of as-received 20 nm nc-Ni

4.1.2 After annealing

XRD profiles obtained after annealing reveal that texture in the material decreases with increasing both annealing time and temperature. Texture above 500 K finally disappears (relative peak intensity decreases from $I_{200/111}$(a) = 0.75 to $I_{200/111}$(d) = 0.46). The effect of annealing temperature on the texture of 20 nm nc-Ni after annealing for a short period of time, i.e. 1 hour, is shown in **Figure 3 (a-d)**. The absence of texture in the material after annealing is shown in **Figure 3 (d)**.

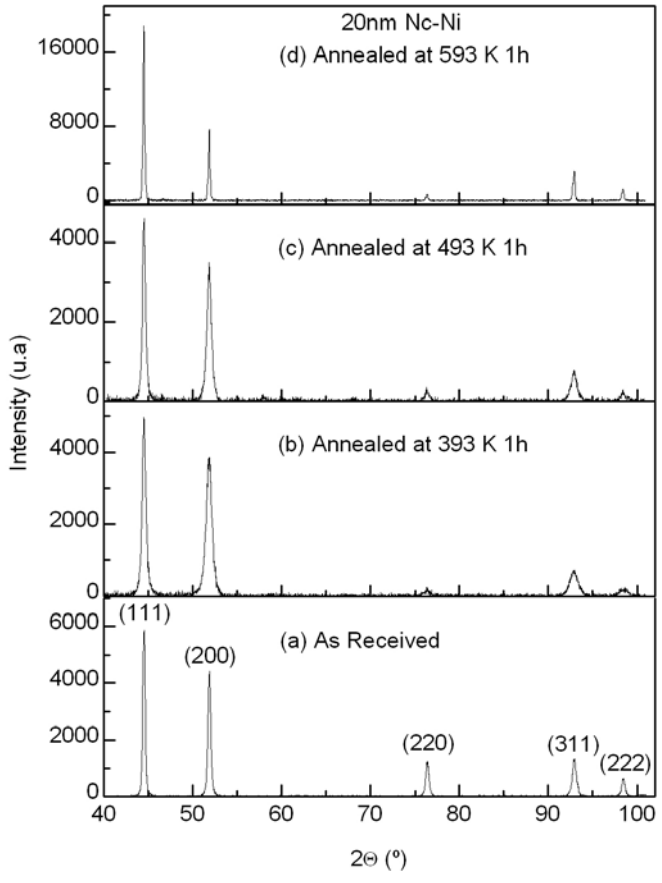

Figure 3 Effect of annealing temperature on the texture of 20 nm nc-Ni.

4.2 Grain size and grain size distribution

4.2.1 As-received

Grain size measurements were performed using the IB method [20], taking into account five FCC diffraction peaks of Ni, i.e. ({111}, {200}, {220}, {311}, and {222}). The average grain size for 15, 20, 25 and 100 nm samples were determined to be 16 ± 2 nm, 18 ± 2 nm, 26 ± 3 nm, and 96 ± 9 nm, respectively. The grain size distribution from transmission electron microscopy (TEM) for 15 and 20 nm samples was previously reported in Ref. [19]. The average grain size obtained from TEM investigation of as-received nc-Ni samples agreed well with those estimated from XRD.

4.2.2 After annealing

TEM and IB method were also used to calculate the average grain size for annealed samples. **Table 2** shows the comparison of the average grain size obtained by both methods.

Sample	XRD	TEM	Grain size Distribution
As-received	18 ± 2 nm	18.1 ± 10.71 nm	Normal. No GG
Annealed at 393 K 1h	20.5 ± 2 nm	20.8 ± 10.07 nm	Normal. No GG
Annealed at 393 K 25h	26 ± 2 nm	31.5 ± 19.05 nm	Bimodal. Abnormal GG
Annealed at 443 K 25h	27 ± 3 nm	46.3 ± 23.88 nm	Bimodal. Abnormal GG
Annealed at 493 K 1h	22 ± 2 nm	38.8 ± 27.17 nm	Bimodal. Abnormal GG
Annealed at 593 K 1h	26 ± 2 nm	322. 9 ± 156.89nm	Normal. GG

Table 2 Grain size values of 20 nm nc-Ni obtained by XRD and TEM methods

XRD and TEM methods showed good agreement on their calculated mean grain size values for samples as-received and annealed at low temperature for a short period, in which a normal distribution was found. However, deviation on the mean grain size values was detected when a bimodal grain size distribution with abnormal grain growth was observed. Furthermore, results obtained from XRD analysis were not reliable at higher temperatures because of evidence of grain growth; grain sizes larger than 100 nm were noted.

Figure 4 (a and b) shows the TEM micrographs for 20 nm nc-Ni samples annealed at 443 K for 25 h and 493 K for 1 h, conditions that represent the annealing temperatures and times of the maximum hardness values obtained by indentation, and **Figure 4 (c)** shows the TEM micrograph of large grain sizes obtained when samples were annealed at 593 K for 1 h. Histograms of their respective grain size distribution, which were calculated using at least 250 grains, are shown in **Figure 5 (a-c).**

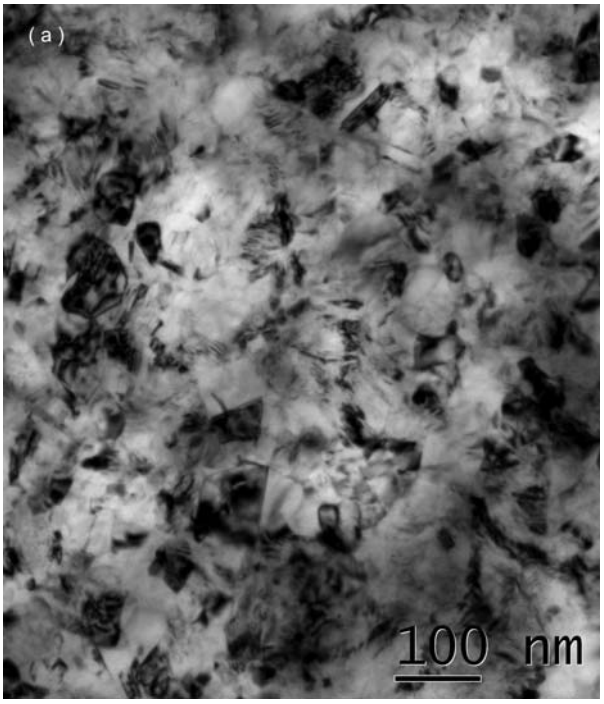

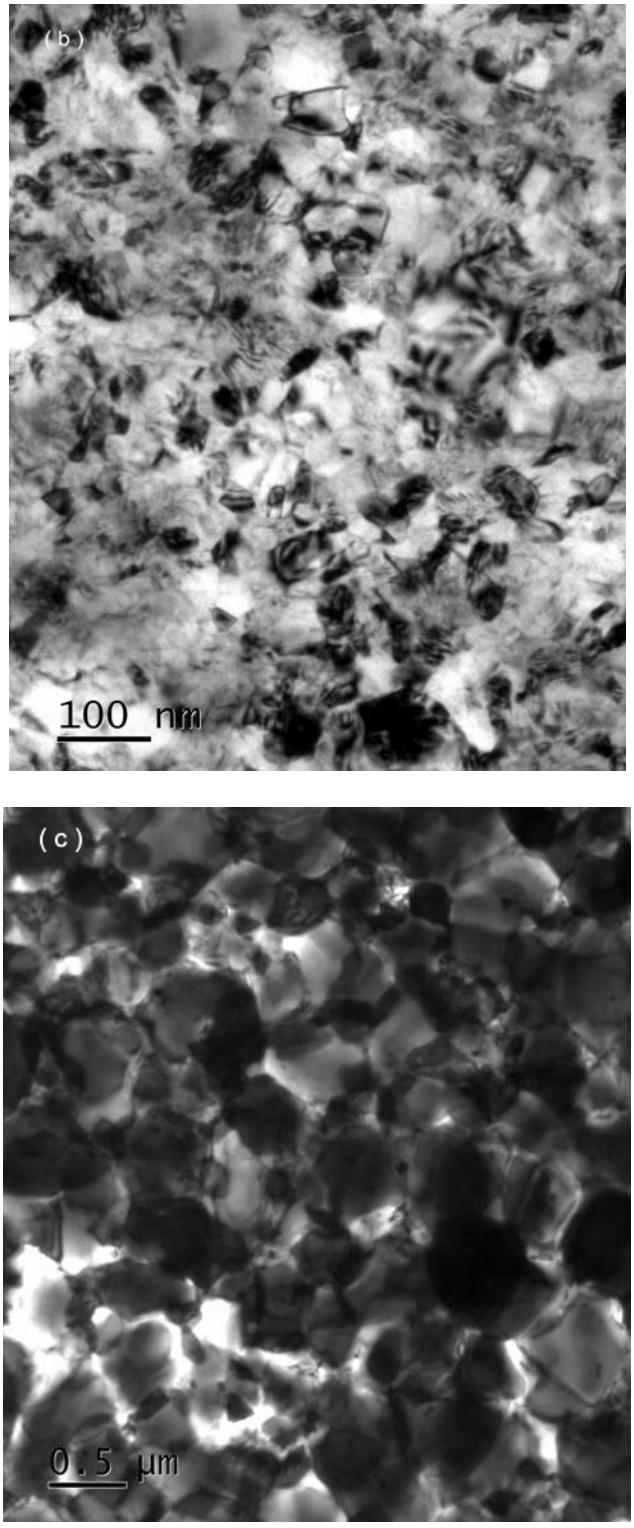

Figure 4 TEM micrographs of 20 nm nc-Ni annealed at: (a) 443 K for 25h, (b) 493 K for 1h, and (c) 593 K for 1h.

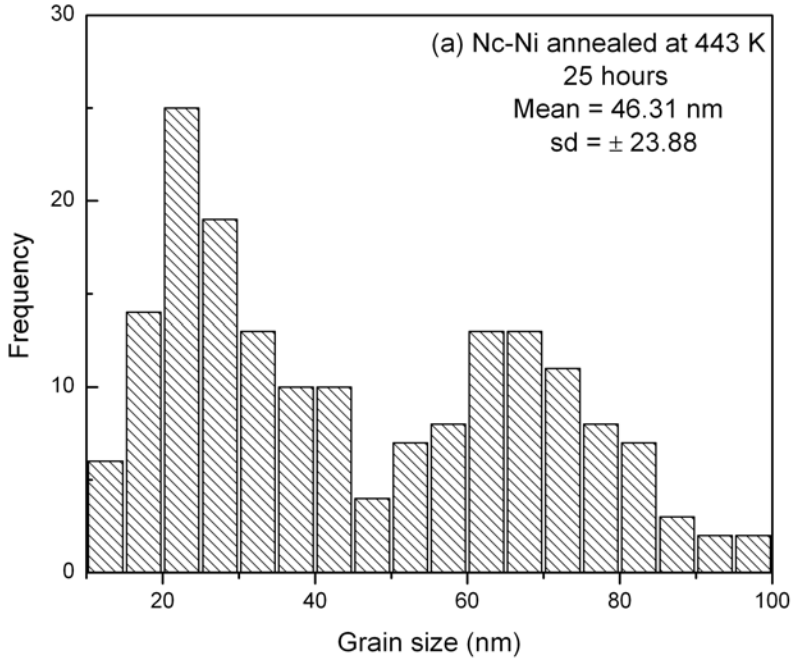
(a) Nc-Ni annealed at 443 K
25 hours
Mean = 46.31 nm
sd = ± 23.88
Frequency
Grain size (nm)
0
10
20
30
20
40
60
80
100

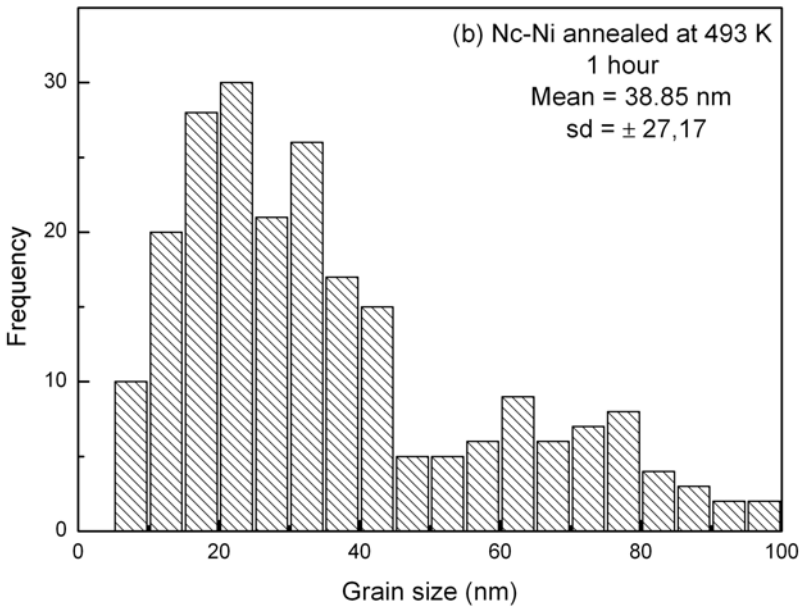
(b) Nc-Ni annealed at 493 K
1 hour
Mean = 38.85 nm
sd = ± 27,17
Frequency
Grain size (nm)
0
10
20
30
0
20
40
60
80
100

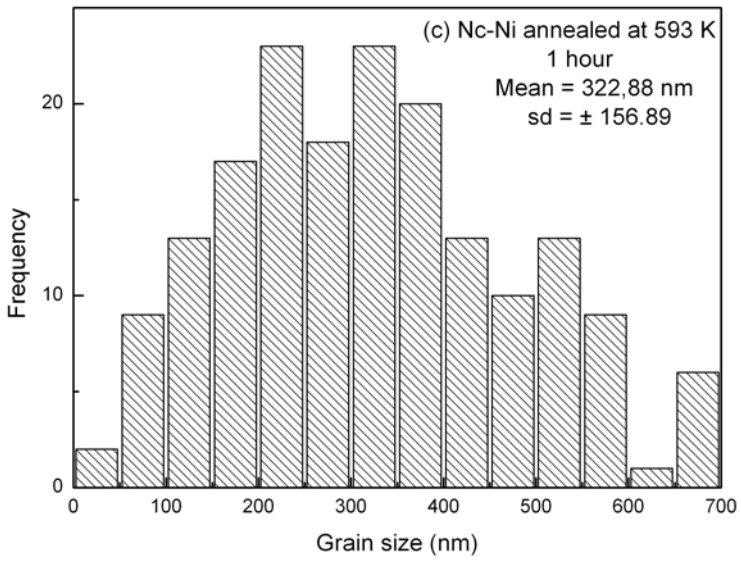

Figure 5 Histogram of 20nm nc-Ni annealed at: (a) 443 K for 25 h, (b) 493 K for 1h, and (c) 593 K for 1h.

4.3 Hardness

4.3.1 As-received

Figure 6 shows the plot of hardness (*H*) versus the inverse square root of grain size ($d^{-1/2}$) obtained from nanoindentation and microindentation using 10, 50 and 200 g load. Data obtained from both methods was consistent in trend; however, hardness values decreased with increasing load. Hardness values obtained from microindenter testing using 10 g agreed with the trend and magnitude obtained from nanoindenter. The figure reveals that hardness data of as-received samples followed a normal Hall-Petch (HP) behavior.

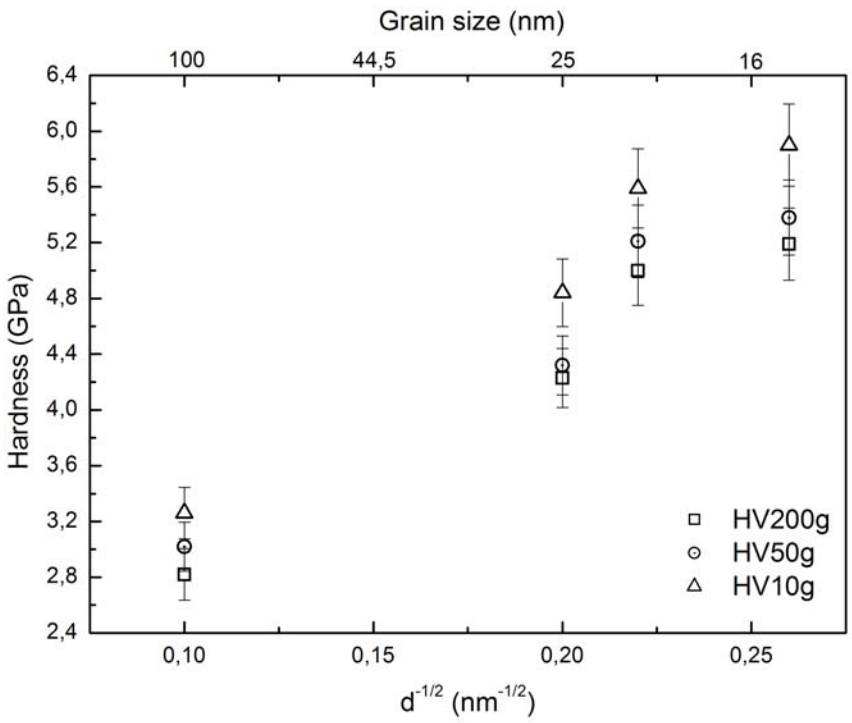

Figure 6 HP plot of experimental HV data when 10, 20, and 200 g load were applied.

4.3.2 After annealing

When nc-Ni samples were annealed at different holding times in the temperature range of 323 – 693 K, the following observations were noted: (a) below 500 K, the hardness slightly increased - one-way Anova statistical analysis at the 0.05 level showed that the population means at 393 K and 493 K were significantly different – until it reached its maximum value; and (b) above 500 K, hardness decreased from the very beginning of the annealing. The change in hardness with annealing temperature after 1 and 25 hours of annealing for 20 nm nc-Ni samples is shown in **Figure 7.**

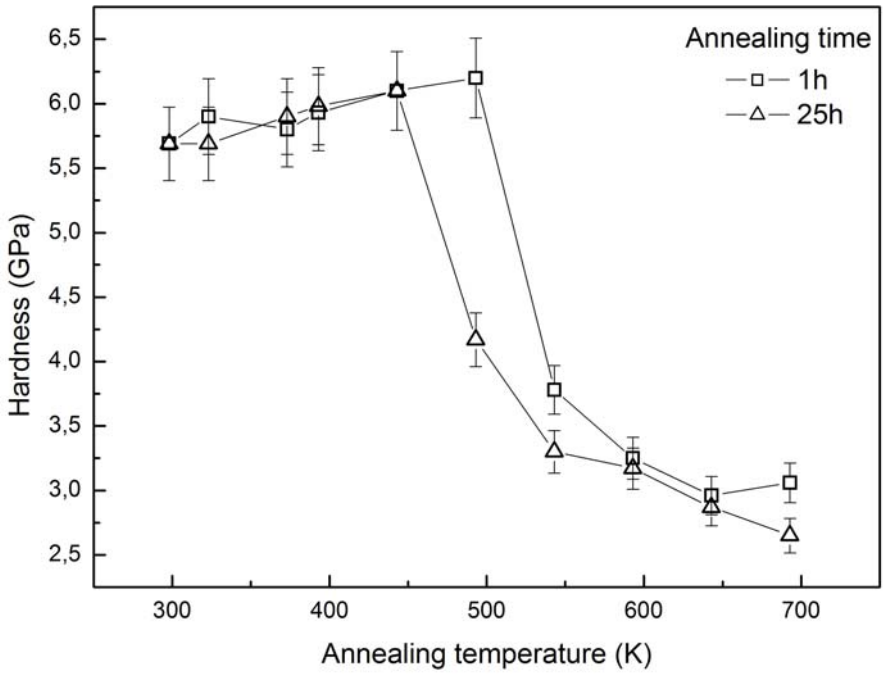

Figure 7 Effect of annealing temperature on hardness

Based on the mean grain size values determined by TEM method, in **Figure 8**, data of as-received and annealed samples obtained using 10 g load on a microindenter is plotted as Hall-Petch (HP) plot. The experimental results of as-received samples showed good agreement with a recent model developed by F.A. Mohamed [24] in which normal HP behavior is predicted for grain sizes down to 13 nm. Annealed samples showed a clear deviation in the HP plot, showing Inverse HP behavior. However, presence of annealing twins in the annealed samples was shown to reduce the effective mean grain size value obtained by TEM. For example, samples annealed above 500 K, would have an effective grain size of around 100 nm instead of 320 nm. Thus, annealed hardness values should be

shifted in the HP plot following F.A. Mohamed model.

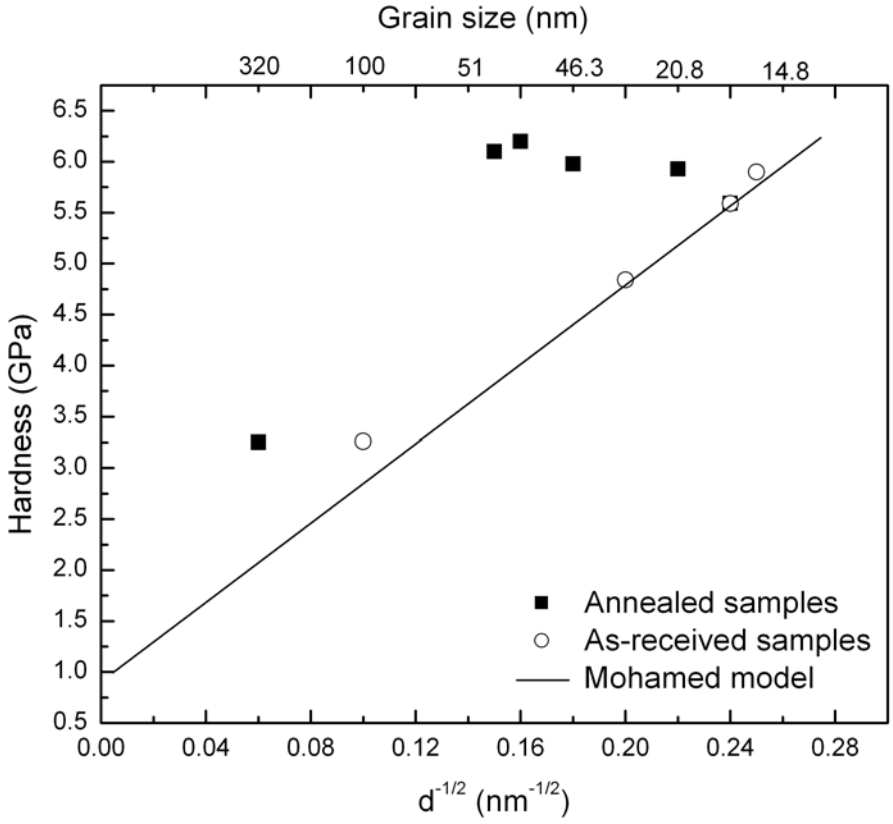

Figure 8 HP plot based on mean grain size values obtained by TEM.

4.4 Young's modulus

4.4.1 As-received

The Young's Modulus (*E*) values for as-received samples plotted as a function of grain size are shown in **Figure 9**. An examination of the figure reveals that the modulus value, *E*, remained almost constant and did not change with grain size, however, the magnitude was much lower (~ 160 GPa) than that reported for coarse grain polycrystalline Ni (207 - 221 GPa) [24, 25].

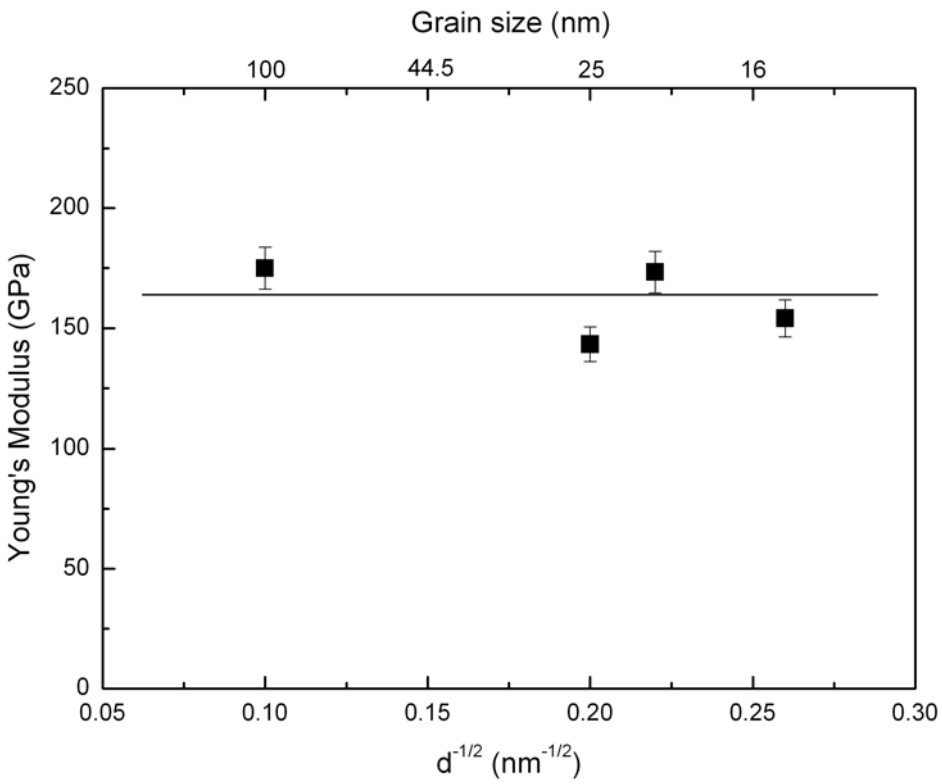

Figure 9 Young's Modulus as a function of grain size.

4.4.2 After annealing

The effect of heat treatment on Young's modulus is plotted in **Figure 10**. The figure shows the change in modulus value for 20 nm samples as a function of annealing temperature after samples were annealed for 25 h. It can be clearly seen that the modulus increased with increasing temperature below 500 K and it remained constant thereafter reaching a maximum plateau around 250 GPa, which is close to the *E* value of coarse grained Ni.

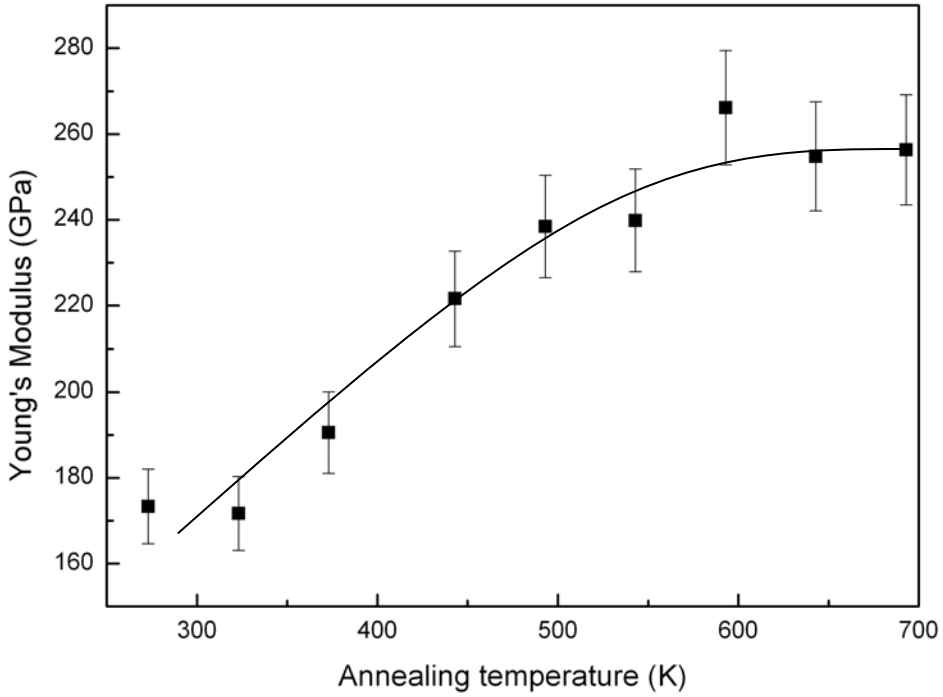

Figure 10 Effect of annealing temperature on Young's Modulus

Young's modulus depends on the orientation of the material. Thus, in a cubic material, such as Ni, the elastic modulus can be determined along any orientation, from the elastic constants, by application of the following equation:

$$\frac{1}{E_{ijk}} = S_{11} - 2\left(S_{11} - S_{12} - \frac{1}{2} S_{44} \right)\left(l_{i1}^2 l_{j2}^2 + l_{j2}^2 l_{k3}^2 + l_{i1}^2 l_{k3}^2 \right) \quad (5)$$

where, E_{ijk} is the Young's modulus in the [ijk] direction; l_{i1}, l_{j2}, and l_{k3} are the direction cosines of the direction [ijk]. Using the elastic compliances for monocrystalline nickel at ambient temperature S_{11} = 0.734x10^{-2}, S_{44} = 0.802x10^{-2}, and S_{12} = -

0.274×10^{-2} GPa^{-1}, E values at [111], [110], and [100] directions are shown in **Table 3**.

	l_{i1}	l_{j2}	l_{k3}	$l_{i1}^2 l_{j2}^2 + l_{j2}^2 l_{k3}^2 + l_{i1}^2 l_{k3}^2$	E_{ijk}
[100]	1	0	0	0	137 GPa
[110]	$\sqrt{2}/2$	$\sqrt{2}/2$	0	$1/4$	232 GPa
[111]	$1/\sqrt{3}$	$1/\sqrt{3}$	$1/\sqrt{3}$	$1/3$	303 GPa

Table 3 Young's moduli along different directions.

The experimental values for as-received nc-Ni showed to be closer to E_{100} than to any other direction, i.e. E_{110} or E_{111}. This result is consistent with XRD profiles in which the preferred texture along (200) planes was also showed.

However, the elastic's modulus increment from 160 to 250 GPa with increasing temperature was attributed to a reorientation of the material, in which the preferred orientation along (200) planes changes to (111) with annealing temperature.

Chapter 5 : Discussion

5.1 Microstructure characterization

The XRD profile of 20 nm as-received ED nc-Ni showed a preferential texture along the (200) planes (**Figure 2**). Similar results on electrodeposited nc-Ni have also been reported by many authors [6, 26-31]. The texture on such samples was mainly attributed to presence of impurities in the electrolyte bath, namely S and C, which seem to enhance the strength of the (100) texture by reducing of the (100) surface energy. Texture was also present in annealed samples (**Figure 3)**. Below 500 K, the preferential orientation along the (200) planes was still in attendance when samples were annealed at different times, i.e. 1 h and 25 h, although it diminished with increasing annealing temperature. Above 500 K, texture was lost, mainly due to grain growth, and random orientated grains were detected. EBSD grain orientation maps agreed with XRD profiles at higher temperature (**Figure 11**).

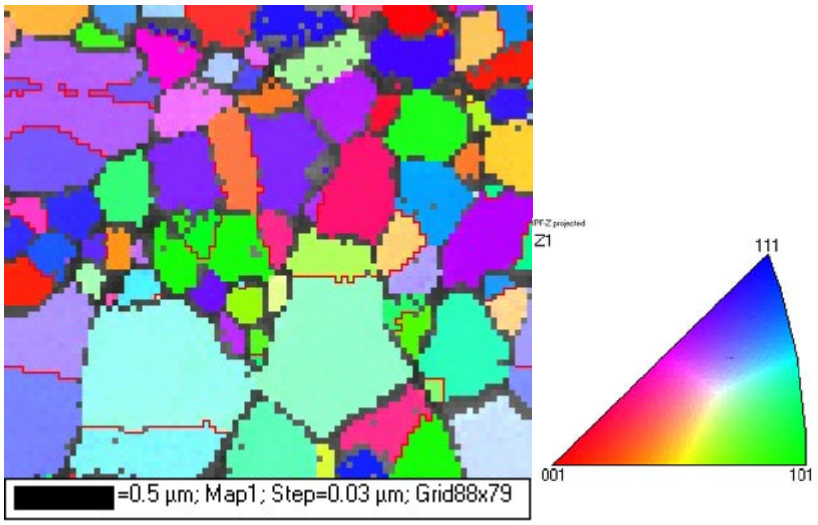

Figure 11 EBSD grain orientation color map of 20 nm nc-Ni annealed at 593 K for 1 h.

XRD and TEM techniques have been always used to compare measurements of grain sizes. Most investigators [19, 32-34] agree with the compatibility of both

methods, although recent studies [26, 35] have demonstrated that grain size measurements from XRD could lead to underestimation when deviations of narrow grain size distributions take place.

In the present study, it is shown that the grain size values of as-received ED nc-Ni samples measured by XRD and TEM were comparable values, while the values obtained from annealed samples were not (**Table 2**). As-received samples showed a good agreement when grain size was compared by both techniques. However, when temperature was increased and different periods of time were applied; reliable results from XRD were not obtained. On the one hand, a bimodal distribution of grain size with wider grain size distribution was detected. On the other hand, there was grain growth and XRD could not give good results because the grain size value obtained at higher temperature was over the limitation of the technique (100 nm).

The grain growth behavior was identified as a two-step process for annealed samples: (a) below 500 K, there was anomalous grain growth and bimodal grain size distributions were detected, and (b) above 500 K, there was normal grain growth. This behavior could be explained as a result of different activation energy for each region. Recent investigation of thermal stability in bulk nc-Ni at low temperature [19] reported two different activation energy values for grain growth. A low energy at temperatures below 0.3 T_m was attributed at reordering boundaries for nc-metals, while the activation energy above 0.3 T_m was higher and closer to grain boundary diffusion activation energy value in polycrystalline Ni. Similar grain growth behavior results were obtained by Klement et al. [31, 36] using differential scanning calorimetry (DSC).

5.2 Annealing twins

Twining can be one of the means to enhance the strength of nc-materials. Usually, deformation twining is observed in FFC metals and alloys with low stacking fault energy, but in severe deformation conditions, twins have also been observed in metals and alloys with higher stacking fault energy. In the present study, twining was observed even when deformation processes were not involved in the experimental procedure (only heat treatments were carried out). Thus, the induced twins observed were originated during the annealing process. TEM micrographs **(Figure 12)** show the presence of annealing twins in those larger grains of samples annealed at 443 K for 25 hrs and 493 K for 1 h, which showed a bimodal grain size distribution. The ultimate effect of twining in large grains is that grains are subdivided into smaller grains, and the effective grain size area is much lower that that initially characterized by TEM. Twining was also observed at temperatures above 500 K during grain growth.

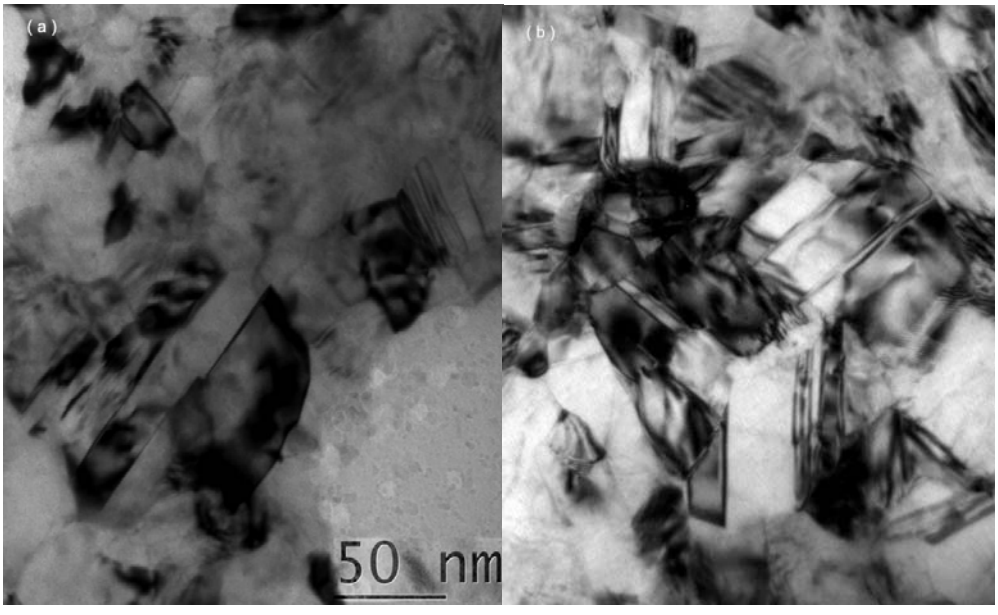

Figure 12 Annealing twins in 20 nm nc- Ni annealed at: (a) 443 K for 25 h, and (b) 493 K for 1 h.

The nature of the boundaries was studied using EBSD. **Figure 13** shows the misorientation maps of a 20 nm nc-Ni sample annealed at 593 K for 1 h. CSL statistics analysis shows that most of the boundaries were $\Sigma 3^n$, of which 65.2% were coherent. Rather than incoherent twins, coherent twins are known to be immobile, blocking dislocation motion to enhance the strength of the material, and resistant to attack and crack initiation.

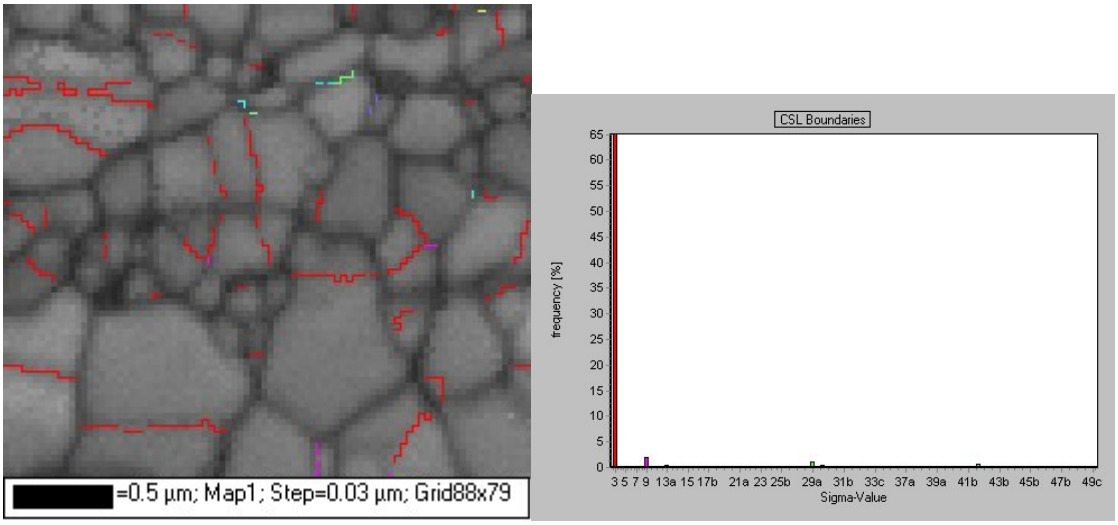

Figure 13 Black and white EBSD grain orientation map showing sigma 3 boundaries in red. Also shown is the CSL statistics of sigma 3 boundaries.

5.3 Hardness and Young's modulus

Hardness results of the nc-Ni samples are shown in **Figure 14**. The HP plot also contains hardness data of nc-Ni from previous studies such as El-Sherik et al. [8], Schuh et al. [7, 9], , Mohamed F.A recent model [37] and Hughes et al. [38], in which nickel was produced by either pulsed current electrodepostion or DC electrodeposition. The first three authors reported a HP break around 20, 14 and 13

nm, respectively, while Hughes et al. reported a normal HP behavior. Although Schuh et al. [9] considered that the differences in grain sizes for inverse HP behavior could be due the fabrication method, a recent model by F.A. Mohamed [37] seems to clarify whether the inverse transition point should be according to a dislocation-accommodated boundary sliding model. Our experimental data of nc-Ni samples, ranging from 15 to 100 nm, accurately fits in his model.

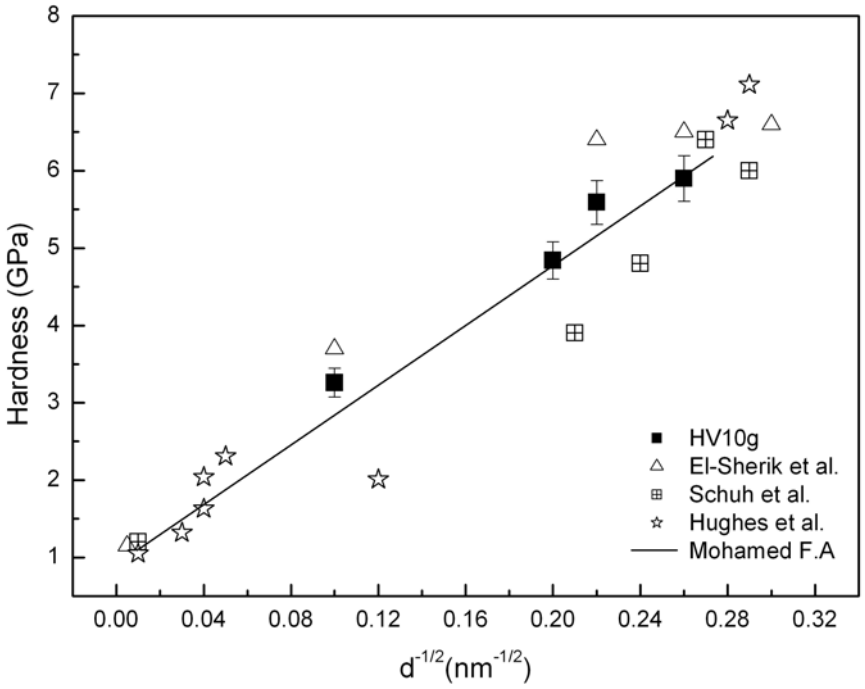

Figure 14 HP plot comparing experimental and reference data.

Besides hardness, the Young's modulus of as-received samples was found to be approximately 160 GPa. According to the XRD profiles (See **Figure 2**), a strong (200) texture was detected in the material and that may be the cause for this reduced value. Fritz et al. [29] also reported a *E* value of 165 GPa when samples

presented a preferential orientation along the (100) planes.

Hardness and Young's modulus data of annealed samples, in the range of 323 - 693 K, reveal the presence of a transition temperature around 500 K. Based on the trends obtained for microindentation and the elastic modulus of nc-Ni after annealing, and together with the results obtained from recent investigation by Chauhan and Mohamed [19] on thermal stability, sample behavior can be divided in two regions according to the annealing temperature: (a) Region I, a low temperature region (T < 500 K), and (b) region II, a high temperature region (T > 500 K).

Region I (low temperature region (T < 500 K): in this region, microhardness increased slightly after heat treatment. According to the XRD data, the as-received ED nc-Ni had a strong (200) texture that decreased with annealing temperature; it fully disappeared after annealing at higher temperatures. In this temperature range, there was no appreciable grain growth, but a bimodal grain size distribution and annealing twins were observed.

The presence of annealing twins combined with the decease in (200) texture and the increase of the elastic modulus indicated the microstructure of as-received nc-Ni approached an equilibrium state, inducing strength in the material, by annealing at T < 500 K. Recent studies via molecular dynamic simulation by Hasnaoui et al. [18] have demonstrated that when an annealed sample is close to a more equilibrium structure, initial atomic activities upon subsequent loading becomes less, leading to strengthening i.e., grain boundary (GB) relaxation and triple junction migration (TJ) induce strengthening.

Region II high temperature region (T > 500 K): in this region, microhardness

decreased from the very beginning of the annealing. The value of the elastic modulus reached a maximum plateau that was close to the value of the coarse-grained Ni. In this temperature range, according to the results by several researchers [10, 19, 31, 36], there is a rapid grain growth and the material is no longer remaining in the nanocrystalline range. As a result, softening occurs. Also, noteworthy were hardness values at higher temperatures. Although the calculated mean grain size for annealed samples was around 320 nm, their hardness values were comparable to those of 100 nm specimens, due to the occurrence of annealing twins, also detected at higher temperature.

Chapter 6 : Conclusions

After the annealing of fully dense electrodeposited nc-Ni samples in the temperature range of 323 K to 693 K for various holding times the following observations can be made:

1. The presence of (200) texture in the nc-Ni samples decreased with increasing annealing time and temperature. It fully disappeared after annealing at higher temperatures (T > 500 K).
2. The bimodal distribution of grain size was obtained during heat treatment at low temperatures (T < 500 K), extent of which increased with the increase in temperature.
3. The material's behavior was divided in two different regions based on the annealing temperature. In the low temperature region (T < 500 K), both hardness and elastic modulus increased with increasing temperature. In the high temperature region (T > 500 K), an increase in the annealing temperature resulted in the reduction of hardness value, whereas, *E* remained constant at the maximum value.
4. The strengthening in nc-Ni as a result of annealing in the low temperature range can be attributed to the presence of annealing twins and the occurrence of relaxation at the initially non-equilibrium grain boundaries. Both processes can lead to strengthening. The softening noted at T > 500 was attributed to the occurrence of significant grain growth.

Suggestions for future work

The results of the investigation on the effect of thermal annealing in full dense electrodeposited nc-Ni in wide range of temperatures (393 K – 693 K) provides new information on new mechanisms that may contribute to enhancing the strength of nc-materials after annealing. The following suggestions are made regarding future work:

- Performing an exhaustive grain size's characterization of all the annealed samples by TEM.
- Performing statistical analysis of annealing twins at different temperatures.
- Examining the distance between the annealing twins, and its changes with annealing temperature and time.
- Performing tensile test at different temperatures to corroborate hardness with yield stress values.

References

[1] A. H. Chokshi, A. Rosen, J. Karch, H. Gleiter, Scripta Materialia 23 (1989) 1679-1684.
[2] G. W. Nieman, J. R. Weertman, R. W. Siegel, Journal of Material Research 6 (1991) 1012-1027.
[3] G. W. Nieman, J. R. Weertman, R. W. Siegel, Nanoestructured Materials 1 (1992) 185-190.
[4] J. R. Weertman, Material Science and Engineering A166 (1993) 161-167.
[5] R. W. Siegel, G. E. Fougere, Nanoestructured Materials 6 (1995) 205-216.
[6] F. Ebrahimi, G. R. Bourne, M. S. Kelly, T. E. Matthews, Nanostructured Materials 11 (1999) 343-350.
[7] T. G. Nieh, J. G. Wang, Intermetallics
International Workshop on Ordered Intermetallics and Advanced Metallic Materials 13 (2005) 377-385.
[8] A. M. El-Sherik, U. Erb, G. Palumbo, K. T. Aust, Scripta Metallurgica et Materialia 27 (1992) 1185-1188.
[9] C. A. Schuh, T. G. Nieh, T. Yamasaki, Scripta Materialia 46 (2002) 735-740.
[10] Y. M. Wang, S. Cheng, Q. M. Wei, E. Ma, T. G. Nieh, A. Hamza, Scripta Materialia 51 (2004) 1023-1028.
[11] F. Dalla Torre, H. Van Swygenhoven, M. Victoria, Acta Materialia 50 (2002) 3957-3970.
[12] B. Yang, H. Vehoff, Zeitschrift fur Metallkunde 95 (2004) 499-504.
[13] W. Chen, S. Tien, F. Wu, J. Duh, Surface and Coating Technology 182 (2004) 85-91.
[14] Y. Zhou, U. Erb, K. T. Aust, G. Palumbo, Scripta Materialia 48 (2003) 825-830.
[15] E. O. Hall, Proc. Phys. Soc. 64 (1951) 747-753.
[16] N. J. Petch, Journal of Iron and Steel Institute (1953) 25-28.
[17] G. E. Fougere, J. R. Weertman, R. W. Siegel, S. Kim, Scripta Metallurgica et Materialia 26 (1992) 1879-1883.
[18] A. Hasnaoui, H. Van Swygenhoven, P. M. Derlet, Acta Materialia 50 (2002) 3927-3939.
[19] M. Chauhan, F. A. Mohamed, Material Science and Engineering A 427 (2006) 7-15.
[20] K. P. Kulg, L. E. Alexander, X-ray Diffraction Procedures, John Wiley & Sons, New York, 1974, p. 992.
[21] M. A. Meyers, K. K. Chawla, Mechanical Behavior of Materials, Prentice-Hall International, London, 1999, p. 166.
[22] W. C. Oliver, G. M. Pharr, Journal of Material Research 7 (1992) 1564-1583.
[23] M. F. Doerner, W. D. Nix, Journal of Material Research 1 (1986) 601-609.
[24] Metals Handbook,10th ed.,Vol.2, Properties and selection - Nonferrous Alloys and Special Purpose Materials, ASM International, Materials Park, Ohio, 1990, p.
[25] R. B. Ross, Chapman, Hall '(Ed.)'^'(Eds.)', Metallic Materials Specification Handbook, London, 1992, p.
[26] M. Chauhan, F. A. Mohamed, Journal of Material Science (2006).

[27] F. Dalla Torre, H. Van Swygenhoven, R. Schaublin, P. Spatig, M. Victoria, Scripta Materialia 53 (2005) 23-27.
[28] S. Van Petegem, F. Dalla Torre, D. Segers, H. Van Swygenhoven, Scripta Materialia 48 (2003) 17-22.
[29] T. Fritz, M. Griepentrog, W. Mokwa, U. Schnakenberg, Electrochimica Acta 48 (2003) 3029-3035.
[30] A. M. El-Sherik, U. Erb, J. Page, Surface and Coating Technology 88 (1996) 70-78.
[31] U. Klement, U. Erb, K. T. Aust, Nanostructured Materials
Proceedings of the Second International Conference on Nanostructured Materials 6 (1995) 581-584.
[32] Z. Zhang, F. Zhou, E. J. Lavernia, Metallurgical and Materials Transactions a-Physical Metallurgy and Materials Science 34A (2003) 1349-1355.
[33] H. G. Jiang, M. Rühle, E. J. Lavernia, Journal of Material Research 14 (1999) 549-559.
[34] T. H. De Keijser, J. I. Langford, E. J. Mittemeijer, A. B. P. Vogels, Journal of Applied Crystallography 15 (1982) 308-314.
[35] R. Mitra, T. Ungar, J. R. Weertman, Transactions of the Indian Institute of Metals 58 (2005) 1125-1132.
[36] U. Klement, U. Erb, A. M. El-Sherik, K. T. Aust, Materials Science and Engineering A 203 (1995) 177-186.
[37] F. A. Mohamed, Metallurgical and materials transactions A In Press (2007).
[38] G. D. Hughes, S. D. Smith, C. S. Pande, H. R. Johnson, R. W. Armstrong, Scripta Materialia 20 (1986) 93-97.